Li et al. *Zool. Res.* 2025, 46(2): 285−300
https://doi.org/10.24272/j.issn.2095-8137.2024.266
https://cstr.cn/32248.14.zr.2024.266

ZR | Zoological Research

Article Open Access

Deciphering the genetic basis of sex differentiation in silver-lipped pearl oyster (*Pinctada maxima*) based on integrative transcriptomic analysis

Zi-Jian Li[1,#], Zhi-Hui Yang[1,#], Jia-Hui Wang[1], Yi-Bing Liu[1,2], Hui Wang[1], Ming-Yang Liu[1], Qian-Qian Mu[1], Li-Xia Tang[1], Zhen-Yuan Xu[1], Ping-Ping Liu[1,2,*], Jing-Jie Hu[1,2], Zhen-Min Bao[1,2]

[1] *Key Laboratory of Tropical Aquatic Germplasm of Hainan Province*, *Sanya Oceanographic Institution*, *Ocean University of China*, *Sanya*, *Hainan* 572000, *China*

[2] *MOE Key Laboratory of Marine Genetics and Breeding*, *College of Marine Life Sciences*, *Ocean University of China*, *Qingdao*, *Shandong* 266003, *China*

ABSTRACT

The silver-lipped pearl oyster (*Pinctada maxima*) is the largest and most commercially valuable pearl-producing oyster, renowned for its ability to generate large, lustrous pearls. This species is a sequential hermaphrodite, with pearl production displaying notable sexual dimorphism. Consequently, understanding the molecular mechanisms governing sex determination and differentiation is crucial for advancing breeding strategies in the pearl oyster industry. To elucidate these mechanisms, this study conducted integrative transcriptomic analyses of *P. maxima* gonadal tissues using isoform sequencing (Iso-seq) and RNA sequencing (RNA-seq). Comparative analysis of ovarian and testicular tissues identified 2 768 differentially expressed genes (DEGs). Gene co-expression network analysis delineated four key modules, including three sex-specific modules and one shared module. Key genes implicated in sex determination and maintenance were identified, including *FOXL2*, *NANOS1*, and *β-catenin*, important for ovarian maintenance, and *DMRT*, *SOX30*, *FEM1*, and *FOXJ1*, crucial for testicular maintenance. These genes, widely studied in other taxa, were confirmed as hub genes in the sex-related modules of *P. maxima*. Interestingly, genes within the shared module were significantly enriched in the spliceosome pathway. Alternative splicing analysis highlighted its extensive role in gonadal tissues, with more pronounced activity observed in the testis compared to the ovary. Nearly half (47.83%, 375) of the identified genes undergoing differential alternative splicing (DASGs) also exhibited differential transcript usage (DTUGs), while only 17% of DTUGs overlapped with DEGs. Genes associated with sex differentiation, such as *DMRT*, *β-catenin*, and *U2AF2*, displayed sex-specific and/or sex-biased isoforms. These findings offer novel insights into the molecular basis of sex differentiation in *P. maxima*, which could inform the development of targeted breeding strategies aimed at sex control, thereby enhancing pearl quality and yield in aquaculture. This study offers a robust molecular foundation for advancing breeding programs and optimizing production in the pearl oyster industry.

Keywords: Sex determination/differentiation; Gene network; Alternative splicing; *Pinctada maxima*

INTRODUCTION

Sex differentiation refers to the process by which a bipotential gonad develops into either a testis or an ovary following the determination of sex, a critical mechanism in the reproduction of sexually reproducing organisms. In mammals, the molecular mechanisms of sex determination and differentiation have been well studied. The Y-linked transcription factor *SRY* has been identified as a key regulator, activating *SOX9* to initiate testis differentiation (Koopman, 1999; Sinclair et al., 1990). In the absence of *SRY*, female-specific pathways involving *RSPO1*, *WNT4*, *β-catenin*, and *FOXL2* are activated, giving rise to the ovaries (She & Yang, 2017). Since the discovery of *SRY* in mammals, numerous sex determination genes have been characterized across vertebrates, including *DMY/DMRT1YB*, *DM-W*, and

Received: 14 August 2024; Accepted: 22 November 2024; Online: 23 November 2024

Foundation items: This work was supported by the Hainan Province Science and Technology Talent Innovation Project (KJRC2023A02), Project of Sanya Yazhouwan Science and Technology City Management Foundation (SKJC-KJ-2019KY01) and Sanya Science and Technology Special Fund (2022KJCX91)

[#]Authors contributed equally to this work

*Corresponding author, E-mail: liupingping@ouc.edu.cn

DMRT1 (Bachtrog et al., 2014; Hirst et al., 2018; Li et al., 2022a; Li & Gui, 2018; Matsuda, 2005; Mawaribuchi et al., 2012; Yoshimoto et al., 2008). However, data on the molecular mechanisms of sex determination and differentiation in invertebrates remain limited, particularly in marine mollusks, which exhibit diverse sexual systems (Leonard, 2018) such as gonochorism (e.g., *Patinopecten yessoensis*), simultaneous hermaphroditism (e.g., *Argopecten purpuratus*), and sequential hermaphroditism (e.g., *Pecten maximus*). Recent advancements in high-throughput sequencing technologies have greatly enhanced the sensitivity and depth for life science research (Reon & Dutta, 2016; Wu et al., 2024). Bulk segregation analysis (BSA) and genome-wide association studies (GWAS) have revealed a polygenic sex determination (PSD) system in *Apostichopus japonicus*, with solute carrier family 8 (*SLC8A*) identified as a potential sex-determining gene (Jiang et al., 2024). Previous whole-genome analyses have identified sex-related gene families in the gastropod *Haliotis discus hannai*, including DMRT, TGF-β, and SOX (Zhang et al., 2024). Whole-genome level transcriptomic studies have further identified candidate genes related to sex determination and differentiation in mollusks. Among marine mollusks, *FOXL2* has been demonstrated to play a central role in sex differentiation and ovarian maintenance (Evensen et al., 2022; Fang et al., 2024; Li et al., 2018; Santerre et al., 2012; Teaniniuraitemoana et al., 2015; Wei et al., 2021; Zhang et al., 2014), with various genes, such as *DMRT1L*, *SOX2*, and *SOX30*, found to be essential for spermatogenesis and testicular development in scallops and oysters (Li et al., 2018; Liang et al., 2019; Wu et al., 2020; Zhang et al., 2014).

Alternative splicing (AS), a post-transcriptional regulatory mechanism in eukaryotes, has emerged as a key contributor to sex determination and gonadal differentiation (Gómez-Redondo et al., 2021). In vertebrates, various genes with essential functions in gonadal development and the pathways of sex determination and differentiation, such as *WT1*, *FGFR2*, *LEF1*, *DMRT1*, *CYP19A1*, and *SOX9*, have been shown to undergo AS (Agrawal et al., 2009; Domingos et al., 2018; Gómez-Redondo et al., 2021; Zhao et al., 2018). For instance, in the Indian mugger crocodile (*Crocodylus palustris*), a species with temperature-dependent sex determination, an alternatively spliced isoform of *SOX9* is exclusively detected in female embryos, whereas the unspliced, full-length *SOX9* isoform is expressed in males during the critical temperature-sensitive period (Agrawal et al., 2009), highlighting the involvement of AS not only in genetically driven but also in temperature-dependent sex determination systems. Furthermore, *CLK1/4* has been identified as a temperature-dependent regulator of AS, playing an important role in sex determination in reptiles (Haltenhof et al., 2020). Similarly, in Nile tilapia (*Oreochromis niloticus*), AS of the histone demethylase gene *Kdm6bb* has been shown to govern temperature-dependent sex reversal (Yao et al., 2023). In invertebrates, the role of AS in sex determination has been best characterized in *Drosophila melanogaster* (Hartmann et al., 2011; Ray et al., 2023). A cascade of splicing factors, including an autoregulatory splicing loop controlled by *SXL* (sex-lethal), drives sex-specific expression of *DSX* (doublesex) isoforms and influences sexual differentiation and behavior (Graham et al., 2003). Despite the extensive research on AS in model organisms, studies on marine invertebrates remain limited. Evidence from species such as *Haliotis discus hannai* and *Apostichopus japonicus* suggests that AS plays a role in gonadal differentiation (Kim et al., 2017; Wang et al., 2023), with sex-specific isoforms of genes like *DNAH1* potentially contributing to testicular function or other sex-related processes (Wang et al., 2023).

The silver-lipped pearl oyster (*Pinctada maxima*) (Supplementary Figure S1) is an important tropical aquaculture species, naturally distributed across the central Indo-Pacific region, including Myanmar, Southeast Asia, the Philippines, South China, Australia, and the Solomon Islands (Southgate et al., 2008; Southgate & Lucas, 2008). Renowned for producing high-value, large, lustrous pearls commonly referred to as “South Sea” pearls, *P. maxima* is the largest pearl-producing oyster and is economically vital for global pearl markets (Jones et al., 2013). Together with *P. margaritifera*, it accounts for nearly 50% of the total value of marketed pearls worldwide (Tisdell & Poirine, 2008). Beyond its economic significance, *P. maxima* serves as a sentinel species in the context of global environmental change (He et al., 2024). It exhibits protandrous hermaphroditism (Hart et al., 2016), a form of sequential hermaphroditism common among pearl oysters such as *P. mazatlanica* (Saucedo & Monteforte, 1997), *P. albino sugillata* (Tranter, 1958), *P. fucata* (Hwang, 2007; Kimani et al., 2006), *P. radiata* (Derbali et al., 2009), and *P. margaritifera* (Chávez- Villalba et al., 2011), and typically transitions from male to female after its second year (Hart et al., 2016). Several studies have explored the factors affecting pearl quality (Blay et al., 2017; Gu et al., 2014; Ky et al., 2015; McDougall et al., 2021), revealing that male recipient oysters tend to produce higher-quality pearls compared to females, indicating a correlation between oyster sex and pearl production efficiency (Iwai et al., 2015). Deciphering the molecular mechanisms underlying sex determination and differentiation in *P. maxima* is crucial for establishing genetic improvement programs aimed at enhancing pearl quality or optimizing hatching practices. These improvements rely on better control over gamete and embryo production. Despite its importance, research on the molecular regulation of sex differentiation in *P. maxima* remains scarce.

To gain a comprehensive understanding of sex differentiation in *P. maxima*, this study employed integrative transcriptomic analysis of ovaries and testes using PacBio isoform sequencing (Iso-seq) and short-read RNA sequencing (RNA-seq). A gene co-expression network was constructed, and the genome-wide transcriptomic landscape was analyzed to identify gene-, transcript-, and AS-level features associated with sex differentiation in *P. maxima*. The findings presented in this study provide a comprehensive gonadal transcriptome profile, highlighting post-transcriptional regulatory events and enhancing understanding of the molecular mechanisms underlying sex differentiation in pearl oysters.

MATERIALS AND METHODS

Samples and RNA extraction

Pinctada maxima specimens were obtained from Lingshui, Hainan Province, China. All samples were collected from artificially cultivated, three-year-old, sexually mature pearl oysters in June. Three males and three females were used as biological replicates to ensure the reliability of the results. Male individuals exhibited the following size characteristics: shell height of 14.43±0.25 cm, shell width of 3.1±0.1 cm, shell

length of 15.23±0.42 cm, and weight of 312.31±25.68 g, with a gonadosomatic index (GSI) of 12.74%±1.99%. Female individuals exhibited the following size measurements: shell height of 15.1±1.15 cm, shell width of 3.2±0.2 cm, shell length of 15.33±0.4 cm, and weight of 320.18±30.82 g, with a GSI of 11.83%±1.55%. Dissections were performed on each individual to obtain samples from the gonad (ovary or testis), mantle, gill, hepatopancreas, foot, adductor muscle, smooth muscle, and intestine tissues, resulting in eight distinct samples per individual. These tissues represent primary and readily distinguishable organs of shellfish. Including tissues beyond the gonads allowed for tissue-specific profiling of differentially expressed genes (DEGs) between both sexes. Collected tissues were immediately frozen in liquid nitrogen and stored at −80°C until RNA extraction.

RNA extraction was conducted using TRIzol reagent. RNA concentrations were determined using a NanoDrop2000 spectrophotometer (Thermo Fisher Scientific, USA), and RNA integrity was assessed using an Agilent 2100 Bioanalyzer (Agilent, USA). RNA quality was evaluated by 1.5% agarose gel electrophoresis.

Iso-seq library construction and sequencing

To construct the PacBio Iso-seq library, equal amounts of RNA extracted from nine distinct tissues were pooled. Library preparation followed the Iso-seq protocol, using a Clontech SMARTer PCR cDNA Synthesis Kit (Clontech, USA) and the BluePippin Size Selection System (Sage Science, USA), as described in the Pacific Biosciences protocol (PN 100-092-800-03). The final library was sequenced using the PacBio Sequel platform (Pacific Biosciences, USA).

Iso-seq data processing, gene annotation, and structural analysis

Raw subreads obtained from Iso-seq were preprocessed to generate highly accurate consensus reads (HiFi reads) using circular consensus sequencing (CCS) (--min-passes 1) (Tang, 2019). The HiFi reads were subsequently processed through the IsoSeq3 pipeline (v.3.8.2; https://github.com/PacificBiosciences/IsoSeq), to remove primers, refine sequences, and classify them into full-length (FL), full-length nonchimeric, and clustered reads. The clustered reads were aligned to the reference genome (unpublished data) using minimap2 (v.2.17 -ax splice -t 30 -uf --secondary=no -C5) (Li, 2018). Redundant isoforms caused by 5' RNA degradation were collapsed utilizing the Isoseq3 collapse pipeline (https://isoseq.how/classification/workflow.html), resulting in non-redundant isoforms designated as unique Iso-seq-based transcripts for subsequent analysis.

Functional annotation of the unique transcripts was performed using seven databases: National Center for Biotechnology Information (NCBI) non-redundant protein (NR), EuKaryotic Orthologous Groups (KOG), Swiss-Prot, Kyoto Encyclopedia of Genes and Genomes (KEGG), Protein Family (Pfam), NCBI nucleotide sequences (NT), and Gene Ontology (GO). Annotations for the first five databases were conducted using Diamond (v.0.9.22.123 --more-sensitive -e 1e–5), while NT database annotation was conducted using ncbi-blast-2.12.0 (-evalue 1e–5). GO annotations were derived through UniProtKB ID mapping based on Swiss-Prot results.

To identify non-coding RNAs (ncRNAs) within the transcripts, analyses were performed using open reading frame (ORF) length and GC content (LGC) (v.1.0), coding-non-coding index (CNCI) (v.2.0), and coding potential calculator 2 (CPC2) (v.1.0.1) (Kang et al., 2017; Sun et al., 2013; Wang et al., 2019b). Transcripts unannotated using the Pfam database were integrated with predictions from these tools to compile a set of candidate long non-coding RNAs (lncRNAs).

Structural features of the unique transcripts were analyzed to explore sequence elements and alternative splicing patterns. Simple sequence repeats (SSRs) and alternative polyadenylation were identified using MISA (v.1.0) (Thiel et al., 2003) and TAPIS (v.1.2.1) (Abdel-Ghany et al., 2016), respectively. Fusion genes were detected and classified using cDNA_Cupcake (--min_locus_coverage_bp 500 -d 1000000) and SQANTI3 (v.5.0) (Tardaguila et al., 2018). SUPPA2 (v.2.3) (Trincado et al., 2018) was used to detect all AS events in unique transcripts, including skipped exons (SE), mutually exclusive exons (MXE), retained introns (RI), and alternative 5' and 3' splice sites (A5SS and A3SS).

RNA-seq library construction and sequencing

RNA samples from seven non-gonadal tissues were prepared by combining equal amounts of RNA extracted from one female and one male individual. In total, 27 RNA-seq libraries (nine tissues with three biological replicates each) were constructed. The cDNA libraries were prepared using the NEBNext Ultra™ RNA Library Prep Kit for Illumina (NEB, USA). Following library construction, next-generation sequencing (NGS) was conducted using the Illumina HiSeq NovaSeq platform (Illumina, USA) to generate 150 bp paired-end reads.

RNA-seq data analysis and identification of DEGs in gonads

Raw sequencing reads were subjected to quality control using fastp (v.0.23.4) to generate high-quality reads (Chen, 2023). High-quality reads were then aligned to the *P. maxima* genome (unpublished data) using STAR (v.2.7.11b) (Dobin et al., 2013) with default parameters. Gene and transcript-level raw counts were obtained using stringtie2 (v.1.3.3b). Expression levels were calculated and normalized as transcripts per million (TPM) (Abrams et al., 2019). The DESeq (v.1.10.1) package (Anders & Huber, 2010) was used for differential expression analysis of genes between ovarian and testicular tissues. Unigenes with $Q<0.05$ and $|\log2(\text{FoldChange})|>1$ were considered DEGs.

Gene co-expression network construction and identification of sex-related modules

Weighted gene co-expression network analysis (WGCNA) was conducted to construct gene co-expression networks using the R package, following previously described procedures (Langfelder & Horvath, 2008). Briefly, to ensure robust network construction, genes with low expression levels or small variation across samples were excluded according to the median absolute deviation (MAD) method. Key parameters were optimized based on WGCNA guidelines, with a soft-thresholding power of 22 selected to achieve a scale-free network structure (model fitting index $R^2=0.8$). Spearman correlation coefficients were calculated for gene pairs to generate an adjacency matrix. Hierarchical clustering of all genes was performed based on dissimilarity measure of topological overlap, resulting in a gene dendrogram. Modules were initially detected using the cutreeDynamic method with the parameters minModuleSize=30 and detectCutHeight=0.995. To enhance biological interpretability, the generated

modules were merged using the parameter detectCutHeight= 0.177. Module significance was assessed by calculating gene significance (GS) and module membership (MM) to evaluate the relationship between modules and phenotypic traits. Sex-related modules were identified based on the criteria: coefficient>0.6 and P<0.05. The relationships between traits and modules were visualized using a module-trait relationship heatmap. Furthermore, overrepresentation analysis of DEGs was performed for module refinement using a hypergeometric test. Modules with Q<0.01 and RichFactor>0.2 were considered sex-related.

Enrichment analysis of genes in related modules and hub gene selection

To identify functional pathways and key regulators in related modules, all genes within these modules were visualized using heatmaps. Both GO and KEGG enrichment analyses were performed using GOstats (v.2.26.0) (Falcon & Gentleman, 2007). Pathways significantly enriched compared to the genomic background were defined by a false discovery rate (FDR)≤0.05. Highly connected genes within a module, referred to as hub genes, were identified based on intramodular connectivity (Kin), which measures the strength of the connections between a gene and others in the module. The top 15% of genes with the highest Kin values were designated as hub genes for a given module. The expression levels and sequences of these key genes are provided in Supplementary Table S1.

Validation of key DEGs through real-time reverse transcription quantitative polymerase chain reaction (RT-qPCR)

To confirm the accuracy of key DEGs, six representative genes exhibiting differential expression across groups were selected for RT-qPCR validation. The RNA samples used for RT-qPCR amplification were identical to those used for RNA-seq library construction. For each sample, 1 μg of total RNA was treated with gDNA Eraser (Takara Bio) to eliminate genomic DNA contamination. The purified RNA subsequently served as a template for reverse transcription using a PrimeScript™ Reverse Transcriptase Reagent Kit (Takara, China), following the manufacturer's guidelines. Gene-specific primers (Supplementary Table S2) were designed with Primer (v.5.0) software, and eukaryotic translation elongation factor 1B (*eEF1B*) was used as an internal control. RT-qPCR was carried out on the QuantStudio 5 Real-Time PCR System (Thermo Fisher Scientific, USA) with ChamQ SYBR Color qPCR Master Mix (Vazyme, China), in accordance with the manufacturer's instructions. The reaction conditions included an initial denaturation step of 30 s at 94°C, followed by 40 cycles at 94°C for 5 s and 60°C for 30 s, and a final step at 95°C of 15 s and 60°C for 1 min. The relative expression levels of target genes were determined using the $2^{-\Delta\Delta Ct}$ comparative threshold cycle (Ct) method. All reactions were conducted with three biological replicates, and the resulting Ct values were analyzed using an independent samples t-test in GraphPad Prism (v.10.1.2). Results are presented as means±standard deviation (SD) of triplicates.

Prediction of protein-protein interactions (PPIs) among key sex-related genes

STRING (v.12.0) (https://cn.string-db.org/) was used to predict and identify PPIs among key sex-related genes, using default parameters. Pearson correlation analysis was conducted to assess co-expression relationships among these genes. Results were visualized as heatmaps using the pheatmap package (v.1.012).

Analysis of AS, differential alternative splicing (DAS), and differential transcript usage (DTU) in gonads

AS events were analyzed using rMATs (v.4.1.0) (Shen et al., 2014) based on the alignment results in Section 2.4. Percent spliced in (*PSI*) values were computed for average exon inclusion levels in the gonadal transcriptome, enabling the detection of AS events. These events were categorized into five types: SE, RI, A3SS, A5SS, and MXE. DAS events were identified by the criteria of FDR<0.05 and |IncLevel Difference|>0.1. The output of rMATs was displayed using a sashimi plot (https://github.com/Xinglab/rmats2sashimiplot). The PPI network of DASGs was analyzed using STRING (v.12.0) (https://cn.string-db.org/) with default parameters (Franceschini et al., 2013). Hub genes within the PPI network were identified using the maximal clique centrality (MCC) method via the cytoHubba module in Cytoscape (Chin et al., 2014). For DTU analysis, transcript-level TPM matrices were used as input data. The RATs R package (Froussios et al., 2019) was employed to independently perform DTU calling at both the gene and transcript levels using the G-test of independence.

RESULTS

Comprehensive transcript identification

The full-length transcriptome of *P. maxima* was generated using PacBio Iso-seq, enabling the identification of as many transcripts as possible. The sequencing effort produced 1 478 221 CCS reads derived from 60 819 512 subreads, corresponding to a total of 154.02 Gb of nucleotide data. After primer removal, demultiplexing, and refinement, 1 234 555 full-length non-chimeric fragments were generated, from which 84 867 full-length consensus transcripts were produced by clustering. To remove redundancy, these transcripts were mapped to the reference genome, resulting in 37 838 unique isoforms (Figure 1a), corresponding to 15 137 unique genes (Supplementary Table S3). Most transcripts (25 207, 66.6%) had lengths between 1 kb and 3 kb, with an average transcript length of 2 658 bp (Supplementary Figure S2A). A wide range of isoforms was identified per gene, ranging from 1 to 180 isoforms. Notably, 44.7% of the detected genes (n=6 774) had more than one isoform, with 8.6% (n=1 304) characterized by more than six isoforms (Supplementary Figure S2B). Multi-exon transcripts were significantly longer than mono-exon transcripts, reflecting the complex transcriptome structure (Supplementary Figure S2C). A high proportion of transcripts (48.54%) were characterized as novel not-in-catalog isoforms (NNC: n=18 336) (Supplementary Table S3), a trend consistent across various transcript lengths (Supplementary Figure S2D). Functional annotations of the identified transcripts were performed using seven major databases, including the Nr, KEGG, GO, KOG, SwissProt, Nt, and Pfam databases. Of the unique transcripts, 17 783 (47%) were annotated in all seven databases, while 35 020 (92.55%), 30 405 (80.36%), 25 645 (67.78%), 23 194 (61.30%), 26 281 (69.46%), 30 572 (80.80%), and 29 697 (78.48%) were annotated in the Nr, KEGG, GO, KOG, SwissProt, Nt, and Pfam databases, respectively (Supplementary Figure S3A). The top 10 homologous species are shown in Supplementary

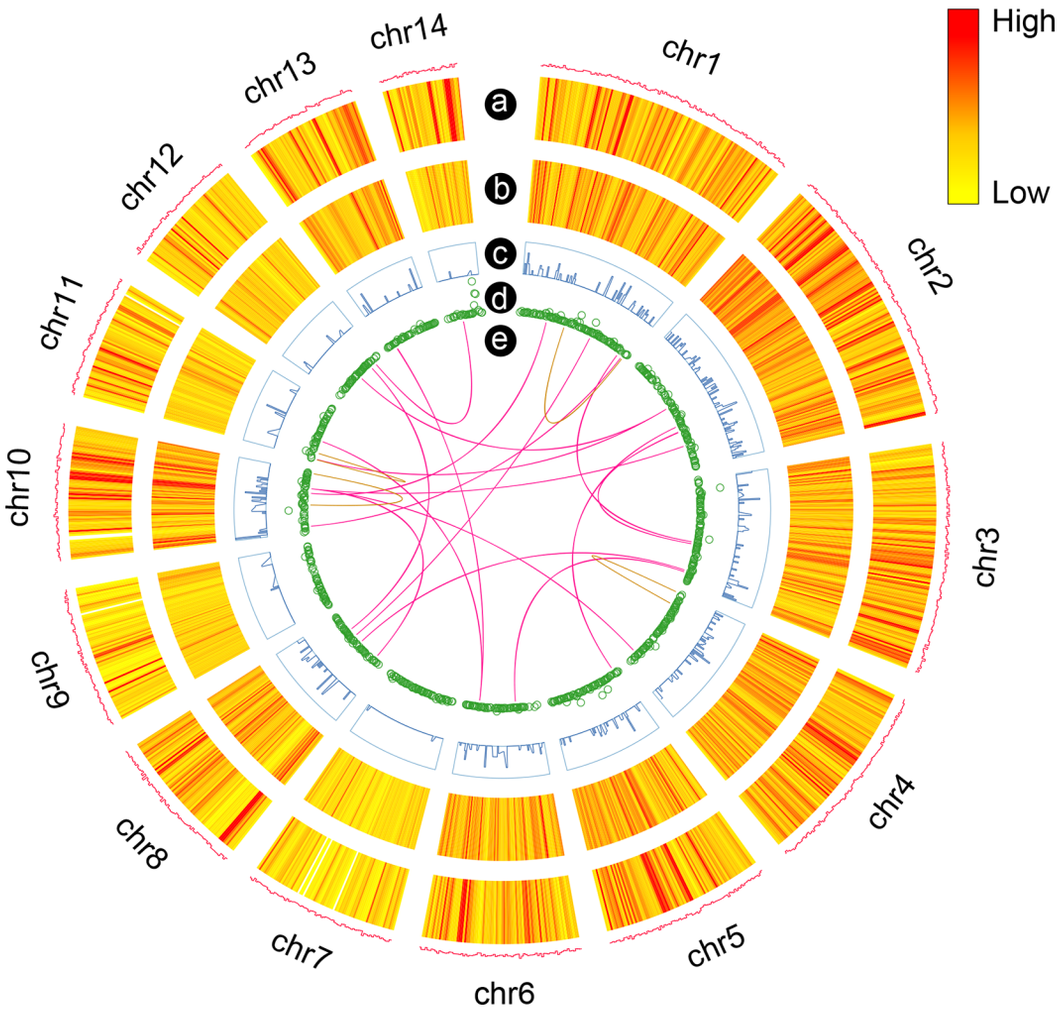

Figure 1 Circos visualization of different data at the genome-wide level

a: PacBio Iso-seq gene (Line) and transcript (Heatmap) density. Gene density was calculated using a 1 Mb sliding window at 100 kb intervals. b: LncRNA density. c: Simple sequence repeat (SSR) density in the genome. d: Transcription factor (TF) density in 1 Mb bins on each chromosome. e: Linkage of fusion transcripts: brown, intra-chromosomal; pink, inter-chromosomal.

Figure S3B, and enrichment analyses were conducted for GO, KOG, and KEGG classifications to provide insights into the functional roles of the transcripts (Supplementary Figure S3C–E).

Transcript characterization

Approximately 90.09% (34 086) of the identified transcripts were predicted to be protein-coding, with an average CDS length of 1 583 nucleotides. Multi-exon transcripts comprised the majority of these, accounting for 34 081 (90%) of the total transcripts (Supplementary Figure S2C). LncRNAs were identified using four computational tools, including CPC2, CNCI, LGC, and Pfam, collectively predicting 19 198 transcripts as lncRNAs (Supplementary Figure S4A). Genomic distribution analysis revealed a notable density of lncRNAs on chromosome 14, particularly in the region chr14: 32 200 000–32 300 000, which contained 244 putative lncRNAs (Figure 1b).

SSRs, ubiquitous across eukaryote genomes, were extensively characterized in *P. maxima*. A total of 15 533 SSRs associated with 10 637 isoforms were identified (Figure 1c), 3 327 of which contained more than one SSR. The lengths of these SSRs ranged from 10 to 869 bp, with an average length of 18.72 bp, while the number of repeat motifs per SSR ranged from 5 to 52 (Supplementary Figure S4B). Mononucleotide repeat motifs (9–12) were the most abundant, followed by dinucleotide and trinucleotide repeats (5–8) (Supplementary Figure S4B).

A total of 3 015 transcripts were predicted to encode transcription factors (Figure 1d), categorized into 69 distinct families. The three largest families were the zf-C2HC transcription factor family (1 163), homeobox transcription factor family (914), and bHLH transcription factor family (602) (Supplementary Figure S4C).

Fusion transcripts, resulting from the abnormal concatenation of two separate genes, were also investigated. A total of 25 fusion transcripts were identified, including 20 inter-chromosomal and five intra-chromosomal fusions (Figure 1e).

Network construction and identification of sex-related modules

To investigate the molecular mechanisms underlying sex determination and differentiation in the pearl oyster, 27 RNA-seq libraries were constructed, representing nine distinct tissues. A total of 1 314 117 940 raw paired-end sequencing reads (150 bp) were obtained, with 1 210 670 134 (92.12%) high-quality reads remaining after quality control. These reads were aligned to the reference genome to quantify gene expression levels. Differential expression analysis between

ovarian and testicular tissues identified 2 768 DEGs (Supplementary Figure S5A), with a higher number of up-regulated genes in the male gonads (*n*=1 781) than in the female gonads (*n*=987). A gene co-expression network was subsequently constructed to identify functional modules associated with sex determination and differentiation. From the 27 transcriptomes, 19 361 annotated genes with a MAD greater than 0 were included in the analysis, resulting in the identification of 24 modules, ranging from 50 to 3 647 genes in size (Figure 2A). To determine which modules were related to sex determination, correlations between module eigengenes (MEs) —representing the principal components of gene expression within each module —and tissue-specific traits were calculated. The darkorange module exhibited the strongest positive correlation with ovarian traits (Pearson r=0.92, *P*=4e–11). Similarly, significant correlations were observed between the green (Pearson r=0.95, *P*=7e–13) and honeydew1 (Pearson r=0.76, *P*=1e–05) modules and testicular traits (Figure 2B). Interestingly, the palevioletred3 module demonstrated a moderate correlation with both ovarian (Pearson r=0.64, *P*=5e–04) and testicular (Pearson r=0.67, *P*=2e–04) traits (Figure 2B). Overrepresentation analysis of DEGs within these modules revealed significant enrichment in three modules (*Q*<0.01, Richfactor>0.2), including the darkorange (*Q*=2.43e–23), green (*Q*=0), and honeydew1 (*Q*=1.56e–03) modules (Figure 2C). Notably,

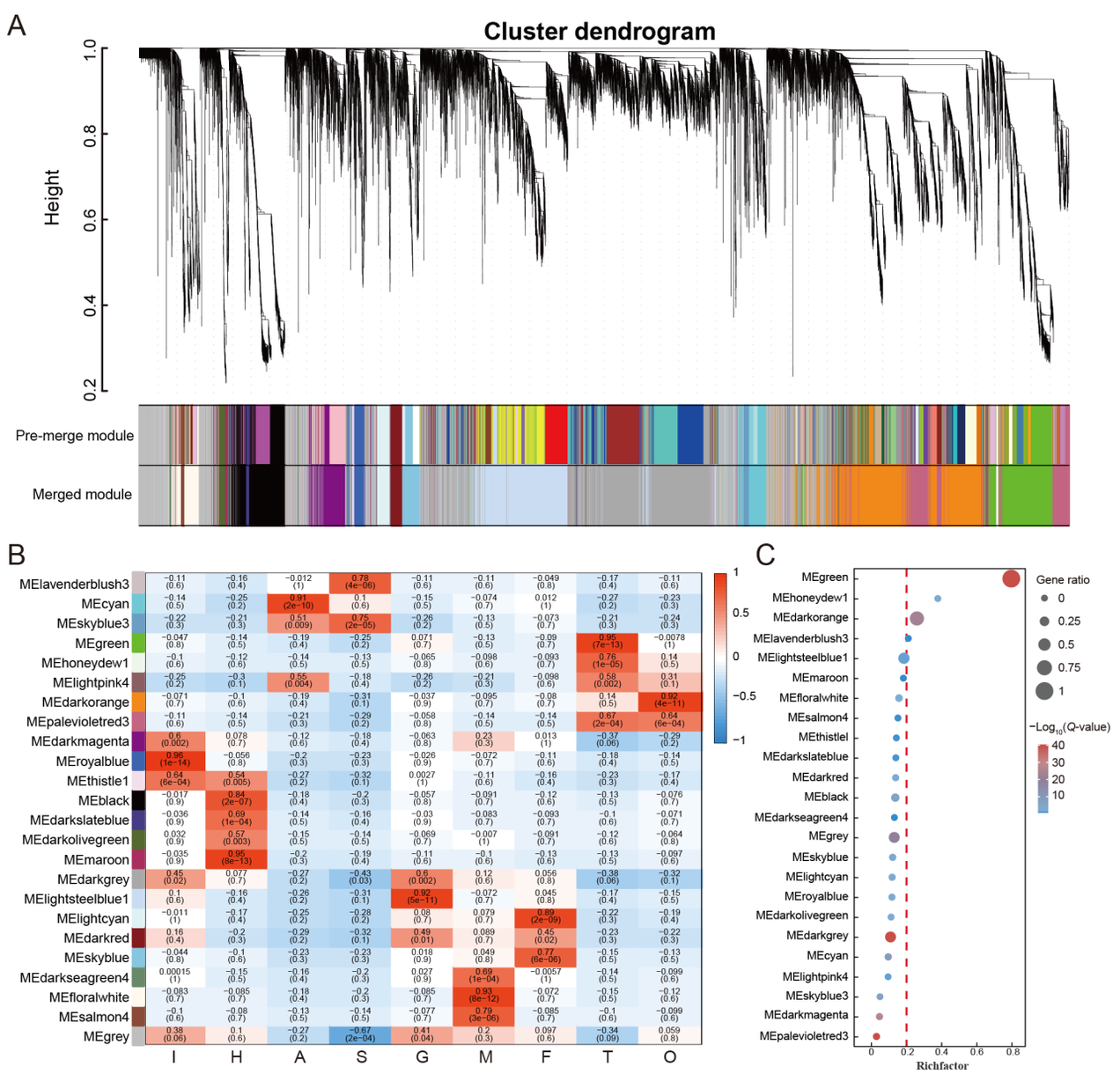

Figure 2 Construction of co-expression network

A: Weighted gene co-expression network analysis (WGCNA) of 27 transcriptomes. B: Module-trait relationships of modules with different tissues. I: Intestine; H: Hepatopancreas; A: Adductor muscle; S: Smooth muscle; G: Gill; M: Mantle; F: Foot, T: Testis; O: Ovary. Red indicates high correlation, blue represents the opposite. Upper numbers in grid represent correlation value. Numbers below in the grid represent significance (*P*-value). C: Overrepresentation analysis revealed that three modules (green, honeydew1, and darkorange) were significantly (*Q*<0.01, RichFactor>0.2) enriched with DEGs. Bubble size represents proportion of enriched genes in the pathway relative to the total number of genes in that pathway, and color represents the magnitude of the *Q*-value, with more intense red indicating more significant enrichment.

these modules contained a high proportion of DEGs, with more than 10% of the genes in each module classified as differentially expressed. The expression profiles of genes within the four sex-related modules were further examined. Results revealed that 2 746 genes in the darkorange module exhibited significantly higher expression in the ovary, while 1 346 genes in the green module and 50 genes in the honeydew1 modules were highly expressed in the testis (Figure 3A; Supplementary Table S4). The palevioletred3 module (1 289 genes) showed high expression in both the ovary and testis, although the expression patterns of some genes were not completely consistent (Figure 3A; Supplementary Table S4). Based on these findings, the darkorange, green, and honeydew1 modules were classified as sex-specific modules, while the palevioletred3 module was classified as a sexually shared module.

Functional annotation of sex-related modules and expression validation of sex-related genes

Functional annotation of sex-related modules was performed using GO and KEGG enrichment analyses to investigate the biological roles of genes within these modules. Genes in the ovary-specific darkorange module exhibited significant enrichment in processes such as regulation of transcription, DNA-templated (*Q*=2.59e–07), progesterone-mediated oocyte maturation (*Q*=6.08e–03), and chromosome organization (*Q*=1.77e–29) (Figure 3B). Hub genes and DEGs identified in this module included forkhead box protein L2 (*FOXL2*), nanos C2HC-type zinc finger 1/nanos homolog 1 (*NANOS1*), nuclear receptor subfamily 2 group E member 1 (*NR2E1*), phosphoribosylaminoimidazole carboxylase and phosphoribosylaminoimidazole succinocarboxamide synthase (*PAICS*), cyclin-H (*CCNH*), GATA zinc finger domain-containing protein 1 (*GATAD1*), DNA replication and sister chromatid cohesion 1 (*DCC1*), cell division cycle protein 23 homolog (*CDC23*), cell division cycle protein 26 homolog (*CDC26*), and sprT-like domain-containing protein Spartan (*SPRTN*), all of which showed significant up-regulation in ovarian tissue (Figure 3C). *β-catenin*, a key component of the WNT/β-catenin signaling pathway, plays a critical role in ovarian development (Chassot et al., 2014). Elevated expression of *β-catenin* was observed in the ovaries of *P. maxima* and other bivalves, such as *Chlamys nobilis* and *Hyriopsis cumingii* (Shi et al., 2018; Wang et al., 2019a). Although *β-catenin* was not included in the darkorange module, likely due to its widespread expression across tissues, it exhibited significant differential expression between the ovary and testis (Figure 3C), suggesting an essential function in sex differentiation in *P maxima*.

The testis-specific green module was enriched in protein binding (*Q*=3.94e–08), cilium organization (*Q*=2.12e–61), and male gamete generation (*Q*=7.47673e–20) (Figure 3B). Representative hub genes and DEGs in this module included doublesex and mab-3 related transcription factor (*DMRT*), feminization-1 (*FEM1*), SRY-box transcription factor 30 (*SOX30*), male-specific lethal 1 homolog (*MSL1*), forkhead box protein J1 (*FOXJ1*), piwi-like RNA-mediated gene silencing 1 (*Piwil1*), piwi-like RNA-mediated gene silencing 2 (*Piwil2*), E2F transcription factor 8 (*E2F8*), coiled-coil domain-containing protein 39 (*CCDC39*), meiosis-specific nuclear structural protein 1 (*MNS1*), cilia- and flagella-associated protein 20 (*CFAP20*), testis-specific serine/threonine kinase (*TSSK*), testis-expressed protein 11 (*TEX11*), and meiotic recombination protein 1 (*DMC1*), all of which are implicated in testicular development. The testis-specific honeydew1 module only contained a small number of genes (50), which precluded enrichment analysis. However, the eight hub genes found in this module included five uncharacterized proteins, two novel genes, and solute carrier family 23 member 1-like (*SLC23A21*). *DMRT* genes, which encode zinc finger DM domains, are pivotal regulators of sex differentiation across a wide range of metazoans, including fish, birds, nematodes, and arthropods (Matson & Zarkower, 2012). In *Apostichopus japonicus*, the gene solute carrier family 8 (*SLC8A*), which encodes the sodium-calcium exchanger (*NCX1*), is a potential candidate gene for determining sex (Jiang et al., 2024). Therefore, *SLC23A21* may be a potential gene for sex differentiation in *P. maxima*.

Six DEGs, including *DMRT*, *SOX30*, *FOXJ1*, *NANOS1*, *FOXL2*, and *β-catenin*, were selected for validation using RT-qPCR. Results confirmed significant expression differences between the testis and ovary, with *NANOS1*, *FOXL2*, and *β-catenin* showing elevated expression in the ovary (P<0.05), and *DMRT*, *SOX30*, and *FOXJ1* exhibiting significant expression in the testis (P<0.05). The high concordance between RNA-seq and RT-qPCR data underscored the reliability of the transcriptomic analysis (Figure 4). PPI network analysis revealed that *FOXL2*, *SOX30*, *PIWIL1*, *PIWIL2*, *NANOS1*, and *TEX11* formed an interaction network (Supplementary Figure S6A). Correlation analysis demonstrated significant associations among *FOXL2*, *NANOS1*, and *PIWIL1* (P<0.001), as well as among *SOX30*, *TEX11*, and *PIWIL2* (P<0.001) (Supplementary Figure S6B).

Genes in the sexually shared module were primarily enriched in pathways related to the mitotic cell cycle (*Q*=1.50e–24), chromatin remodeling (*Q*=1.67e–04), spliceosome (*Q*=4.67e–07), and germ cell nucleus (*Q*=6.03e–09). Hub genes in this module included serine and arginine rich splicing factor 6 (*SRSF6*), U2 small nuclear RNA auxiliary factor 2 (*U2AF2*), heat shock protein family A member 14 (*HSPA14*), small nuclear ribonucleoprotein F (*SNRPF*), DNA topoisomerase II binding protein 1 (*TOPBP1*), and heterogeneous nuclear ribonucleoprotein F (*HNRNPF*). The significant enrichment of the spliceosome pathway further highlights the importance of AS in the sex differentiation of *P. maxima*.

Genome-wide AS events in gonadal transcriptome

Comprehensive analysis of genome-wide AS events of the gonadal transcriptome identified 16 345 AS events from 5 940 genes in the ovary and testis (Supplementary Table S5). To explore the chromosomal distribution of AS events, a heatmap was constructed using a 1 Mb window. Several chromosomal regions exhibited notably high frequencies of AS events, including chr1 (41–42 Mb) with 129 AS events, chr2 (39–40 Mb) with 80 AS events, chr2 (66–67 Mb) with 75 AS events, and chr3 (34–35 Mb) with 96 AS events (Figure 5A). At the chromosomal level, AS events were most frequent on chr2 and chr3, with approximately 24.7 and 19.0 AS events per Mb, respectively, whereas chr7 and chr9 exhibited the lowest frequencies, with 5.2 and 4.9 AS events per Mb (Figure 5A). The identified AS events were classified into five canonical categories, including SE, A5SS, A3SS, MXE, and RI. Among these, SE events were the most prevalent, accounting for 42.9% (7 017 events), followed by A5SS (4 310 events, 26.4%), A3SS (3 429 events, 21.0%), MXE (1 158 events,

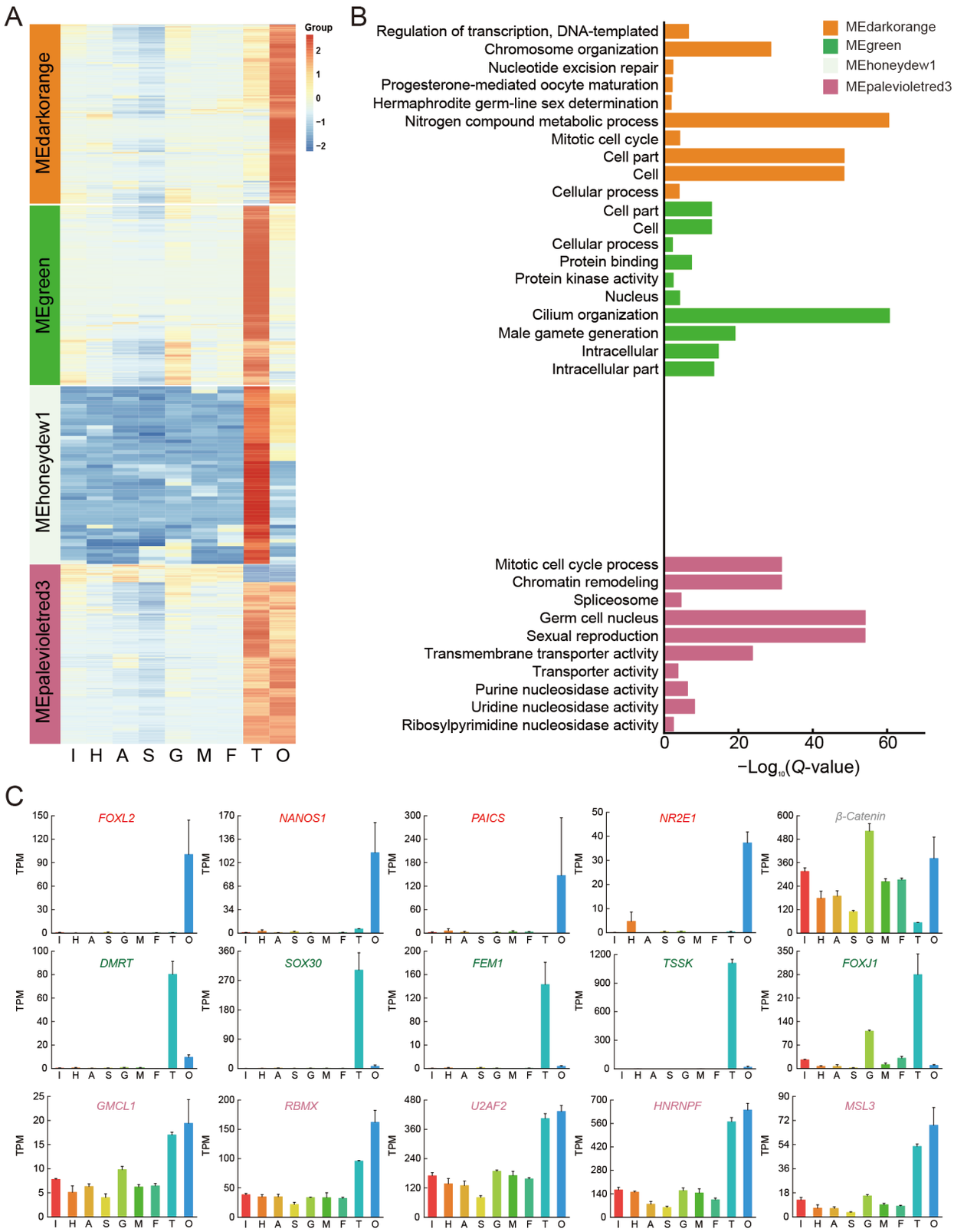

Figure 3 Gene expression pattern and functional enrichment of four sex-related modules

A: Heatmap visualization of all genes in sex-specific (darkorange, green, honeydew1) and shared (palevioletred3) modules. B: GO and KEGG enrichment results of genes in four modules. C: Expression profiles of representative genes from female-specific (darkorange), male-specific (green), and sex-shared module (palevioletred). Gene names are highlighted with corresponding module color. TPM: Transcripts per million.

7.1%), and RI (431 events, 2.6%) (Supplementary Figure S5B). Analysis of tissue-biased AS events revealed 7 185 (44.0%) ovary-biased events, 8 517 (52.1%) testis-biased events, and 643 (3.9%) events with no tissue preference (Figure 5B). The testis exhibited a higher frequency of SE, A5SS, and A3SS events compared to the ovary, whereas ovary-biased AS events were more prevalent in MXE and RI types (Figure 5B).

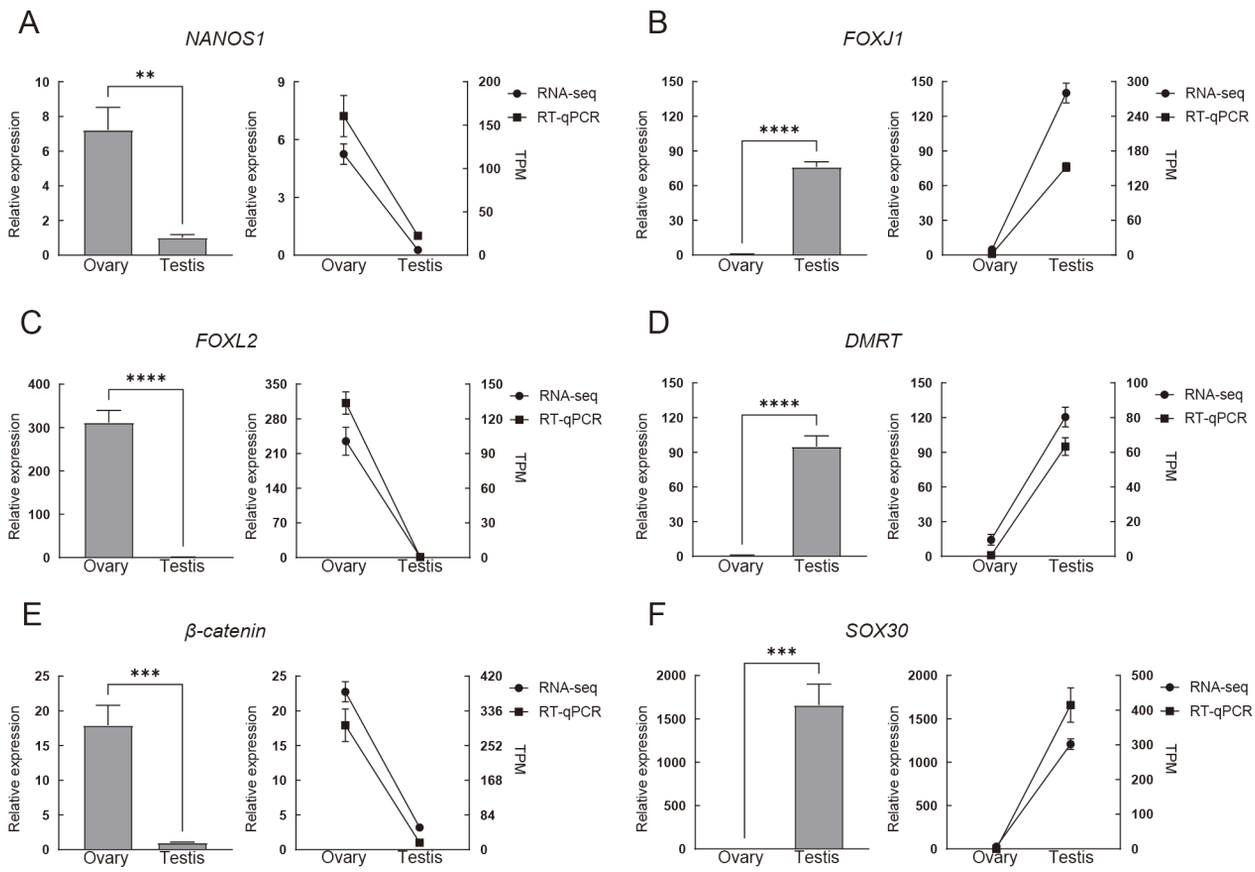

Figure 4 Validation of key DEGs using RT-qPCR and comparison of gene expression patterns

A, C, and E represent up-regulated genes *NANOS1*, *FOXL2*, and *β-catenin* in the ovary; B, D, and F represent up-regulated genes *FOXJ1*, *DMRT*, and *SOX30* in the testis. Error bars represent mean±standard error (n=3). Asterisks indicate significant differences between sexes, *: P<0.05; **: P<0.01; ***: P<0.001; ****: P<0.001. P-value was calculated using the t-test. TPM: Transcripts per million.

DAS between the ovary and testis

Using stringent filtering criteria (FDR<0.05 and |IncLevelDifference|>0.1), a total of 1 351 DAS events were identified across 784 genes in *P. maxima* (Supplementary Table S6). These events were unevenly distributed among the 14 chromosomes, with chr4 exhibiting the highest density (2.0 DAS events per Mb) (Figure 5C). Among these events, the SE, A5SS, A3SS, MXE, and RI types accounted for 58.5% (791), 13.2% (269), 7.5% (178), 19.9% (102), and 0.8% (11), respectively (Supplementary Figure S5D). The patterns of DAS events in the ovary and testis were similar (Figure 5D), with male gonads exhibiting a higher number of up-regulated genes compared to females (Supplementary Figure S5C). GO enrichment analysis of the 784 identified DASGs revealed significant biological processes linked to gametogenesis and reproduction. Notable terms included female gamete generation (Q=2.93e–09), male gamete generation (Q=1.88e–04), and sexual reproduction (Q=5.10e–09). PPI analysis of DASGs revealed one large cluster and several smaller clusters (Figure 6A). Notably, the larger cluster included key splicing and regulatory factors such as RNA binding motif protein X-linked (*RBMX*), U2 small nuclear RNA auxiliary factor 2 (*U2AF2*), polypyrimidine tract-binding protein 1 (*PTBP1*), cell division cycle and apoptosis regulator 1 (*CCAR1*), small nuclear ribonucleoprotein U1 subunit 70 (*SNRNP70*), DEAH-box helicase 15 (*DHX15*), DExH-box helicase 9 (*DHX9*), matrin 3 (*MATR3*), heterogeneous nuclear ribonucleoprotein K (*HNRNPK*), serine and arginine rich splicing factor 6 (*SRSF6*), and serrate RNA effector molecule homolog (*SRRT*), which exhibited strong interactions. Hub DASGs were identified within the PPI network using the MCC method, with the highest ranked genes, such as *RBMX*, *SRSF6*, *DHX9*, *U2AF2*, *SNRNP70*, *SRSF6*, and *HNRNPK*, highlighted as critical regulatory nodes (Figure 6B).

AS regulates genes involved in gonadal differentiation

AS of precursor RNA, along with alternative transcript start- and stop sites, generates multiple transcript isoforms from a single gene. Changes in the relative expression of these isoforms under certain conditions can significantly influence differentiation processes. DTU analysis, which evaluates proportional differences in transcript expression within a gene, provides critical insights into the contribution of each transcript to total gene expression across varying conditions (Froussios et al., 2019). In this study, 4 262 DTU transcripts were identified, corresponding to 2 485 DTU genes (DTUGs) (Supplementary Table S7). Analysis revealed that 998, 1 267, 189, 32, and nine DTUGs contained one, two, three, four, and five DTU transcripts, respectively. Among these, 447, 757, 134, 29, and eight DTUGs underwent a primary switch in transcript usage. Notably, nearly half (47.83%, 375) of the previously identified DASGs (784) were also DTUGs (Figure 6C), underscoring the regulatory influence of AS on gene expression. Among these 375 genes, 89 were DEGs and 71 were hub genes (Figure 6C), further emphasizing the pivotal role of AS in sex differentiation. Interestingly, only 17.63% of DTUGs were differentially expressed at the gene level (Figure 6C), indicating that reliance on DEGs alone may

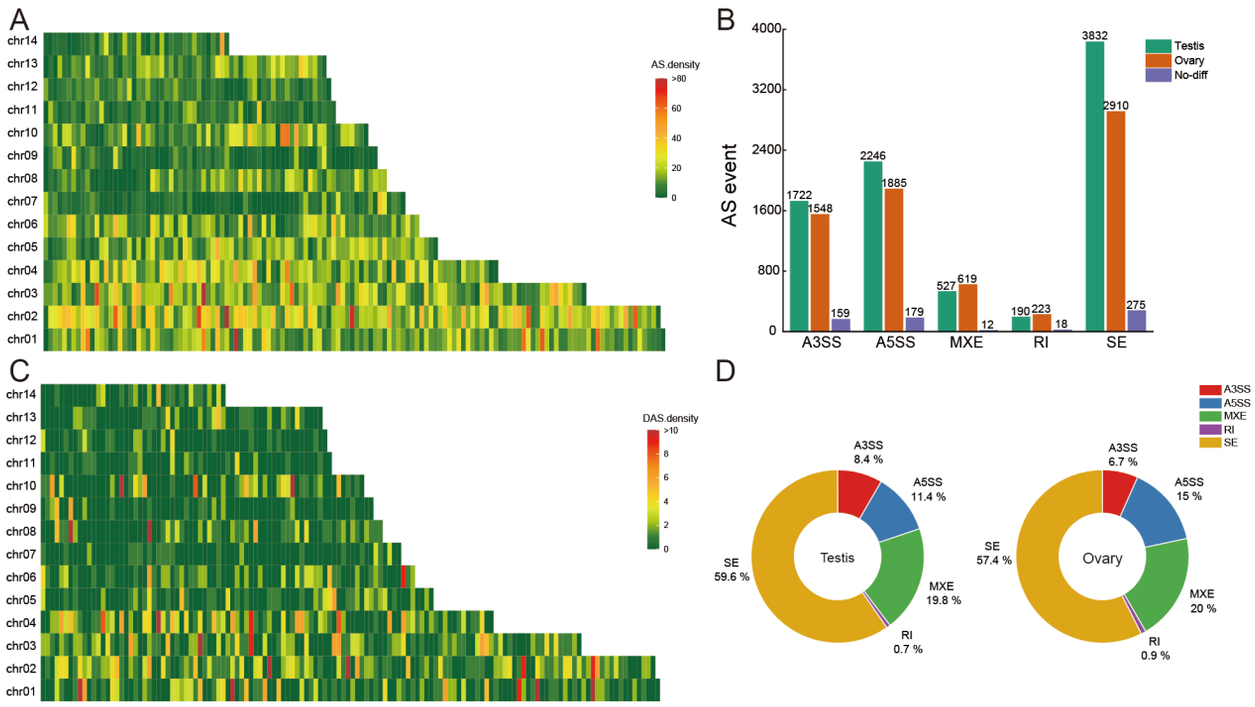

Figure 5 Analysis of AS and DAS in ovary and testis of *Pinctada maxima*

A: Distribution of AS events in chromosomal-level genome. B: Type distribution of AS in ovary and testis. C: Distribution of DAS events in chromosomal-level genome. D: Type distribution of DAS in ovary and testis. Heatmap frequency was calculated with a 1 Mb bin. Green and red indicate low and high frequency AS events in 1 Mb bin, respectively. AS: Alternative splicing; DAS: Differentially alternative splicing; SE: Skipped exon; A5SS: Alternative 5' splice site; A3SS: Alternative 3' splice site; MXE: Mutually exclusive exons; RI: Retained intron.

overlook critical transcript-level dynamics, necessitating DTU analysis. Key sex-related genes, including *DMRT*, *β-catenin*, *U2AF2*, *HNRPNF* and *RBMX*, exhibited sex-specific and/or sex-biased isoforms (Supplementary Table S8). *DMRT* was significantly up-regulated in the testis compared to the ovary (Figure 3C), and two testis-specific transcripts, TCONS_00010611 and TCONS_00010612, were exclusively expressed in the testis (Figure 7A). However, the expression levels of these transcripts were notably lower than TCONS_00016607, which exhibited DTU between the testis and ovary. Although there was no significant difference in the overall gene expression level of *U2AF2* (Figure 3B), differentially expressed transcripts were identified between the ovaries and testes, with the testis-preferred transcript undergoing splicing, resulting in the exclusion of the sixth exon through a SE event (Figure 7B). *β-catenin* was significantly up-regulated in the ovary compared to the testis (Figure 3C), with two ovary-biased transcripts identified (TCONS_00077077 and TCONS_00075940) (Figure 7C). These transcripts differed in their start and end positions, with 34 853 447–34 885 561 for TCONS_00077077 and 34 853 452–34 885 559 for TCONS_00075940, with variation in the utilization of the first exon (Figure 7C).

DISCUSSION

The silver-lipped pearl oyster (*P. maxima*) serves as a sentinel species for monitoring global environmental changes (He et al., 2024) and holds significant economic importance as the largest pearl-producing oyster. However, its sequential hermaphroditism, wherein individuals mature as males and progressively transition to females after approximately two years, poses unique challenges. This reproductive strategy complicates broodstock conditioning for aquaculture and directly impacts pearl production, with male oysters often yielding higher commercial value pearls compared to females. Thus, understanding the molecular mechanisms underlying sex differentiation is crucial for advancing genetic improvement programs aimed at enhancing pearl quality and optimizing hatchery success. Iso-seq, leveraging single-molecule real-time sequencing technology, allows the generation of full-length transcripts without assembly, direct resolution of isoform structure, and interrogation of repetitive RNA sequences (Haile et al., 2021; Wisecaver & Hackett, 2010; Yang et al., 2021). This approach has been extensively employed across diverse species for refining genome-wide gene annotations and exploring AS landscapes (Chen et al., 2022; Guo et al., 2023; Leung et al., 2021; Li et al., 2017; Wang et al., 2016). Despite its advantages, the technology is hindered by high error rates and limited throughput, which constrain its utility in accurately quantifying isoform abundance (Au et al., 2013). To address these limitations, hybrid approaches have emerged, combining long, error-prone reads from third-generation sequencing platforms with short, accurate reads from second-generation sequencers, enabling error correction and enhancing the precision of isoform quantitation (Li et al., 2014). This study identified a transcript-level regulatory network underlying gonadal differentiation through the integration of Iso-seq and RNA-seq analyses.

To gain a comprehensive understanding of the molecular mechanisms and key regulatory drivers underlying sex differentiation, WGCNA was conducted using 27 transcriptomes derived from nine distinct tissues. WGCNA is a robust analytical method that identifies significant gene modules and core regulators within modules, with its efficacy demonstrated in many organisms, including mollusks (Fu et al., 2014; Li et al., 2022b; Rurak et al., 2022; Sabik et al.,

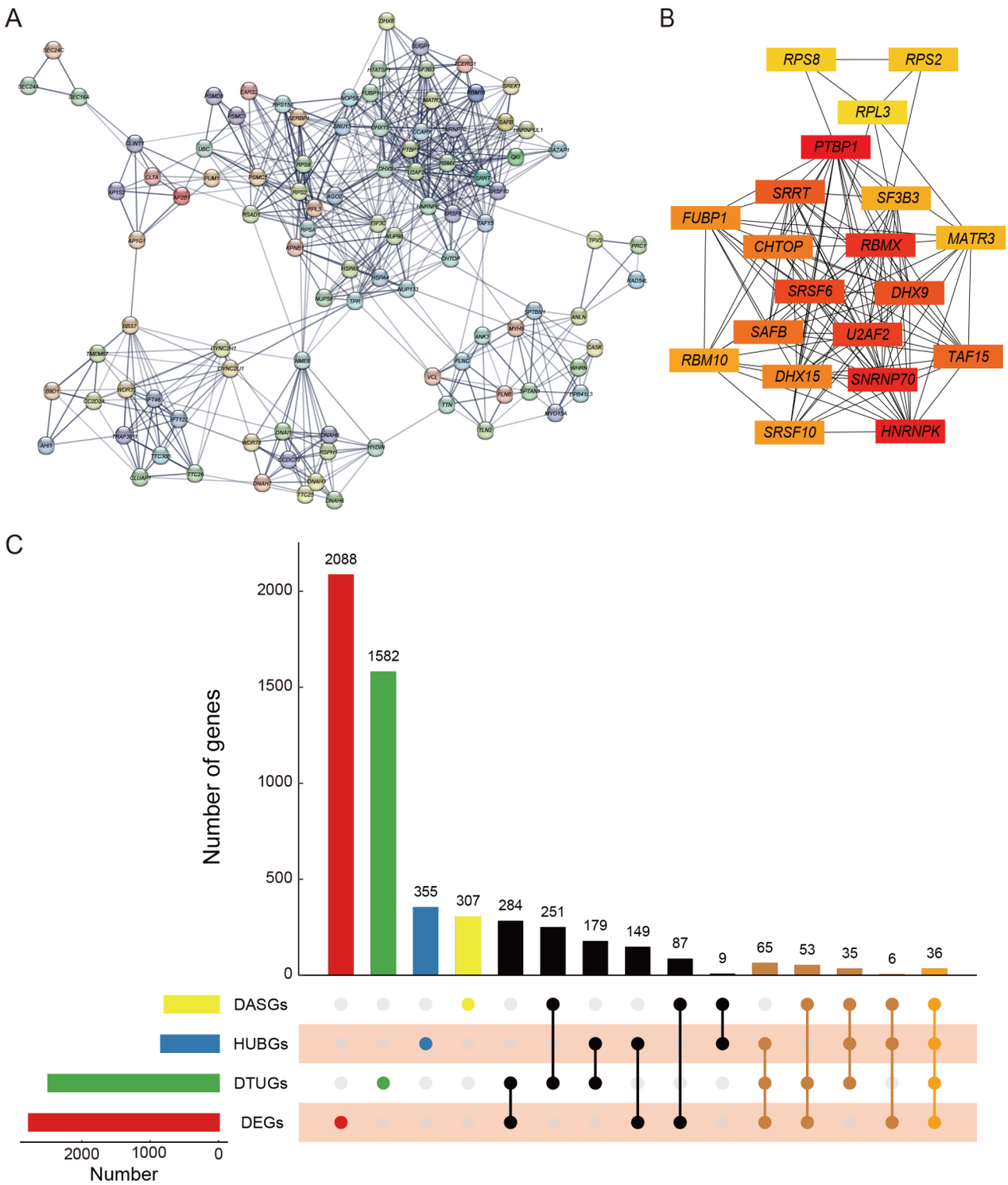

Figure 6 Analysis of DASGs in *Pinctada maxima*

A: Protein-protein interaction (PPI) network analysis of differential alternative splicing genes. B: Identification of core genes based on maximal clique centrality (MCC) score. Red represents high connectivity in the network, yellow represents low connectivity in the network. C: UpSet plot of interaction relationships among DASGs, HUBGs, DTUGs, and DEGs. DASGs: Differential alternative splicing genes; HUBGs: Hub genes; DTUGs: Differential transcript usage genes; DEGs: Differentially expressed genes.

2020; Xu et al., 2021; Zhang et al., 2012). This analysis identified three sex-specific modules and one sexually shared module. Notably, the darkorange module was significantly enriched in hermaphrodite germ-line sex determination, chromosome organization, and mitotic cell cycle, while the green module was significantly enriched in cilium organization and male gamete generation and the palevioletred3 module was significantly enriched in mitotic cell cycle, spliceosome, germ cell nucleus, and sexual reproduction. These findings are consistent with prior studies reporting analogous gene sets associated with sex differentiation-related GO terms in bivalves and other species (Capt et al., 2019; Deng et al., 2022; Li et al., 2022b; Tong et al., 2015; Wang et al., 2022).

Through integrative analysis of hub genes in co-expression

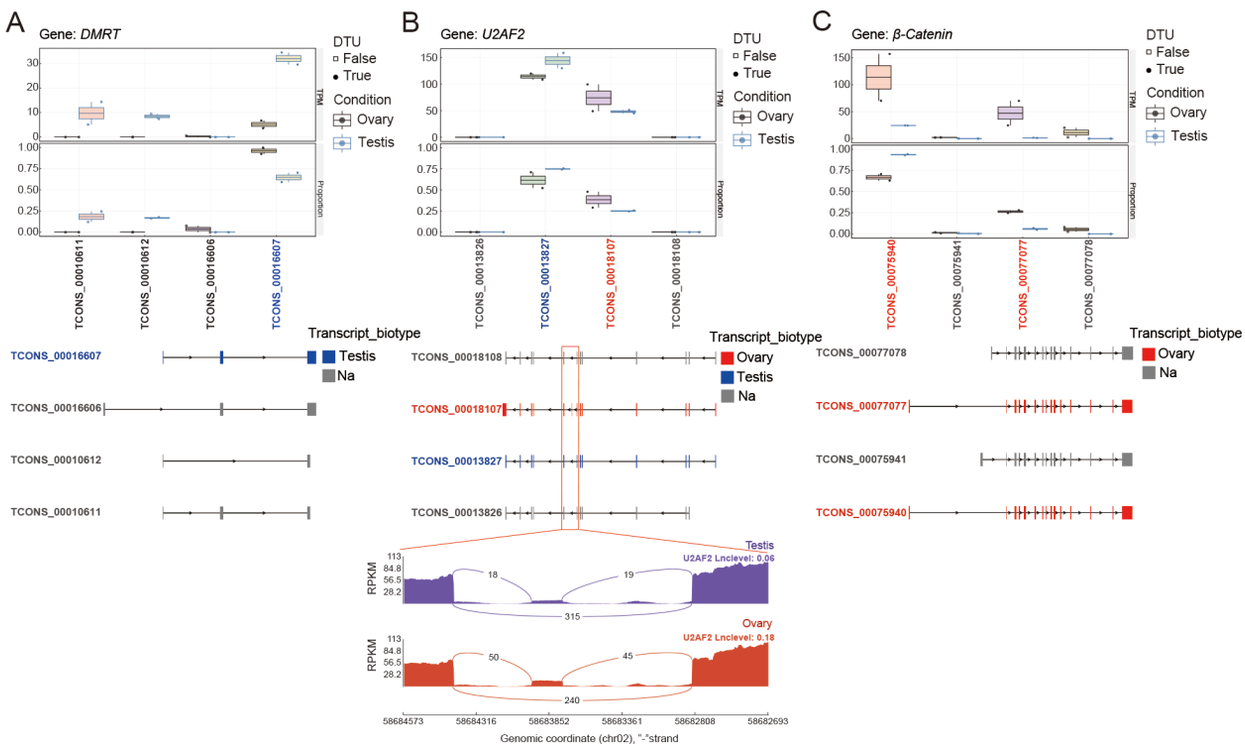

Figure 7 DTU and DAS analysis of genes with sex-specific isoforms

A: DTU analysis of *DMRT*. B: DTU and DAS analyses of *U2AF2*. C: DTU analysis of *β-catenin*. DTU: Differential transcript usage. Boxplot represents expression levels of different transcripts, with dots indicating transcripts differentially used in two tissues. In the transcript structure diagram, blue represents transcripts up-regulated in the testis, red represents transcripts up-regulated in the ovary. Red box indicates position of alternative splicing events.

modules and DEGs, this study identified multiple key regulators of gonadal development in *P. maxima*. Among these, *FOXL2*, *NANOS1*, and *β-catenin* were important for ovarian maintenance, while *DMRT*, *SOX30*, *FEM1*, and *FOXJ1* were crucial for testicular function and maintenance (Figure 3C). *FOXL2* is highly conserved across vertebrates and invertebrates, serving as a critical regulator of ovarian differentiation (Bertho et al., 2016), with its expression observed in various mollusks (Evensen et al., 2022; Li et al., 2018; Teaniniuraitemoana et al., 2015; Wei et al., 2021; Zhang et al., 2014). *NANOS* is essential for the differentiation and migration of primordial germ cells, contributing to their fate in multiple species (Kobayashi et al., 1996; Lai et al., 2012). In bivalves, *Nanos* genes such as *PyNanos1* and *PyNanos2/3* have been identified in *Patinopecten yessoensis*, where they are specifically expressed in germ cells, implying key roles in gametogenesis (Liu et al., 2022). Similarly, Cg-Nanos-like in *Crassostrea gigas* is involved in germ cell development and oocyte maturation (Xu et al., 2018). The elevated expression of *NANOS1* in the ovary of *P. maxima* highlights its conserved role in oocyte development, paralleling its function in *Crassostrea gigas*. *β-catenin*, a key component of the WNT/β-catenin signaling pathway, is critical for ovarian development (Chassot et al., 2014). Its up-regulation in the ovary has also been observed in other bivalves, such as *Chlamys nobilis* and *Hyriopsis cumingii*, where it is crucial for ovarian maintenance (Shi et al., 2018; Wang et al., 2019a). *DMRT* genes encode zinc finger DM domains and are central to sex differentiation across metazoans, including fish, birds, nematodes, and arthropods (Matson & Zarkower, 2012). In mollusks such as *Patinopecten yessoensis* and *Pinctada margaritifera*, *DMRT* genes exhibit sexually dimorphic expression (Li et al., 2016; Teaniniuraitemoana et al., 2015). *FEM1* is a component of the sex determination signaling pathway in *Caenorhabditis elegans* (Doniach & Hodgkin, 1984). In pearl oysters, *FEM1* is thought to contribute to male development and spermatogenesis (Teaniniuraitemoana et al., 2014). *SOX30* is implicated in mammalian spermatogonial differentiation and spermatogenesis (Ballow et al., 2006; Osaki et al., 1999), with functional loss leading to arrested spermatogenesis (Feng et al., 2017). In mollusks, such as *Octopus sinensis*, *Patinopecten yessoensis*, *Haliotis discus hannai*, and *Crassostrea gigas*, *SOX30* exhibits sexually dimorphic expression (Li et al., 2016, 2024; Zhang et al., 2014, 2024). *FOXJ1*, essential for ciliogenesis and motile cilia biogenesis, is associated with sperm motility in mammals (Beckers et al., 2020). Its male-biased expression in mollusks like *Octopus sinensis* suggests a role in sperm flagella development and male differentiation (Li et al., 2024). PPI network analysis indicated potential interactions among *FOXL2*, *SOX30*, *PIWIL1*, *PIWIL2*, *NANOS1*, and *TEX11*. Notably, strong correlations were observed among *FOXL2*, *NANOS1*, and *PIWIL1*, as well as among *SOX30*, *TEX11*, and *PIWIL2*. In vertebrates, an interaction between *FOXL2* and *SOX9* has been previously identified (Baddela et al., 2023). As *SOX30* belongs to the same family as *SOX9* but exhibits distinct gonadal expression patterns, it is possible that *FOXL2* interacts with *SOX30*. However, further research is needed to uncover the molecular basis of this potential interaction.

AS has emerged as a pivotal regulatory mechanism in sex determination and gonadal differentiation (Gómez-Redondo et al., 2021; Lu et al., 2022), supported by its significant enrichment in the spliceosome pathway of the sexually shared module. Several pre-mRNA splicing factors, such as *RBMX*

and *U2AF2*, identified within this module, have been previously implicated in sex determination and differentiation (Elkrewi et al., 2021). These findings underscore the essential role of AS in modulating sex-specific processes. AS has been extensively studied in various species, revealing its critical function in generating isoforms of key sex-related genes, including *SRY*, *DMRT1*, *SOX9*, and *Cyp19a1* (Agrawal et al., 2009; Albrecht et al., 2003; Domingos et al., 2018). In this study, abundant AS events were identified in *P. maxima* gonadal tissues, with SE events representing the predominant type, consistent with patterns observed in other species (Huang et al., 2016; Zhang et al., 2019). Male gonads contained a higher number of DEGs undergoing DAS compared to female gonads, indicating a more dynamic AS process in testicular tissues. Previous research has shown that the permissive chromatin environment in testes facilitates the emergence of novel genes, particularly in spermatocytes and sperm cells (Kaessmann, 2010). Our results indicated that the *P. maxima* testis may possess a more sophisticated array of post-transcriptional regulatory mechanisms. Key genes associated with sex differentiation were found to have sex-specific and/or sex-biased isoforms, including *DMRT*, *β-catenin*, *U2AF2*, *RBMX*, *HNRNPF*, and *MSL3*. Notably, two testis-specific isoforms and one testis-biased transcript of *DMRT* were identified in *P. maxima.* In chickens, *DMRT1* undergoes AS to produce multiple transcripts, such as DMRT1a (elevated in male gonads at stage 31), *DMRT1c* (higher in female gonads), and *DMRT1g* (specific to male gonads at stage 31), each playing distinct roles in gonadal differentiation (Zhao et al., 2007). Similarly, in the ricefield eel (*Monopterus albus*), four *DMRT1* isoforms have been identified in adult gonads. Of which, two splice forms, *DMRT1a* and *DMRT1b*, showing increased expression during the transition from ovaries to testes (Huang et al., 2005). Given that *P. maxima* also undergoes sex reversal, it remains to be determined whether *DMRT* contributes to this process. Two ovary-biased isoforms of *β-catenin* were identified in this study, suggesting a role in ovarian development, though its isoform-level regulation in other species remains unknown. *U2AF2*, a known splicing factor, did not exhibit differential gene expression between sexes, yet sex-preferred isoforms were observed, highlighting its potential involvement in gonadal function. Further research is needed to elucidate the roles of these isoforms in the ovary and testis of *P. maxima.* Recent studies have demonstrated that manipulating AS pathways can directly influence sex determination and even achieve sex reversal through targeted manipulation of spliceosome components (Gregoire et al., 2023; Van't Hof et al., 2024; Yao et al., 2023). Such findings emphasize the potential for AS-driven regulatory interventions in sex differentiation. Environmental stressors, such as marine heatwaves, have significantly impacted marine ecosystems, leading to mass mortality events among invertebrates and posing a threat to wild *P. maxima* populations (He et al., 2024). As a protandrous hermaphrodite with sequential sexuality, *P. maxima* faces inherent restrictions in population expansion. Understanding the molecular basis of sex regulation is therefore crucial for their conservation and aquaculture. Comparative genomic analyses have revealed localized differences across linkage groups between male and female pearl oysters (Jones et al., 2013), providing a foundation for the development of sex-related markers and breeding strategies. This study provides new insights into isoform-level sex-related markers and potential strategies for sex control, which could enhance breeding programs and support the conservation of *P. maxima* populations.

CONCLUSIONS

This study advances our understanding of the molecular mechanisms underlying sex differentiation in the silver-lipped pearl oyster. Integrative transcriptomic analyses at the gene, transcript, and AS level identified key regulators of gonadal differentiation in *P. maxima.* Crucial genes such as *FOXL2*, *NANOS1*, and *β-catenin* were found to play pivotal roles in ovarian development, while *DMRT*, *SOX30*, *FEM1*, and *FOXJ1* were crucial for testicular development. Notably, AS was shown to be extensively distributed throughout the genome of *P. maxima*, underscoring its important role in sex differentiation. Key genes, including *DMRT*, *β-catenin*, and *U2AF2*, exhibited sex-specific or sex-biased isoforms, highlighting their potential importance in the regulation of sex differentiation and reversal. Further functional studies are required to elucidate the detailed regulatory networks involving *DMRT*, *β-catenin*, and *U2AF2*, particularly their roles in sexual reversal mechanisms. The identification of isoform-specific markers in these genes offers promising avenues for developing molecular markers for sex identification and manipulating sex determination. These findings have significant implications for improving breeding strategies and enhancing pearl yield in *P. maxima*, contributing to the conservation and sustainable aquaculture of this economically and ecologically important species.

DATA AVAILABILITY

The sequencing data obtained in this study have been uploaded to the Science Data Bank database (SDB, Data DOI: 10.57760/sciencedb.j00139.00125), Genome Sequence Archive database (GSA, accession number: CRA020554), and National Center for Biotechnology Information database (NCBI, BioProjectID: PRJNA1187804).

SUPPLEMENTARY DATA

Supplementary data to this article can be found online.

COMPETING INTERESTS

The authors declare that they have no competing interests.

AUTHORS' CONTRIBUTIONS

P.P.L., Z.M.B., and J.J.H. designed the experiments and supervised the study. Y.B.L. performed the sampling. Z.J.L., Z.H.Y., Q.Q.M., H.W., and Z.Y.X. carried out the experiments. Z.J.L., Z.H.Y., L.X.T., J.H.W., and M.Y.L. performed the computational framework and analyzed the data. Z.J.L., Z.H.Y., and P.P.L. wrote the manuscript. P.P.L. and Z.M.B. revised the manuscript. All authors read and approved the final version of the manuscript.

REFERENCES

Abdel-Ghany SE, Hamilton M, Jacobi JL, et al. 2016. A survey of the sorghum transcriptome using single-molecule long reads. *Nature Communications*, **7**: 11706.

Abrams ZB, Johnson TS, Huang K, et al. 2019. A protocol to evaluate RNA sequencing normalization methods. *BMC Bioinformatics*, **20**(S24): 679.

Agrawal R, Wessely O, Anand A, et al. 2009. Male-specific expression of *Sox9* during gonad development of crocodile and mouse is mediated by alternative splicing of its proline-glutamine-alanine rich domain. *The FEBS Journal*, **276**(15): 4184–4196.

Albrecht KH, Young M, Washburn LL, et al. 2003. *Sry* expression level and

protein isoform differences play a role in abnormal testis development in C57BL/6J mice carrying certain *Sry* alleles. *Genetics*, **164**(1): 277–288.

Anders S, Huber W. 2010. Differential expression analysis for sequence count data. *Genome Biology*, **11**(10): R106.

Au KF, Sebastiano V, Afshar PT, et al. 2013. Characterization of the human ESC transcriptome by hybrid sequencing. *Proceedings of the National Academy of Sciences of the United States of America*, **110**(50): E4821–4830.

Bachtrog D, Mank JE, Peichel CL, et al. 2014. Sex determination: why so many ways of doing it?. *PLoS Biology*, **12**(7): e1001899.

Baddela VS, Michaelis M, Tao XL, et al. 2023. *ERK1/2-SOX9/FOXL2* axis regulates ovarian steroidogenesis and favors the follicular-luteal transition. *Life Science Alliance*, **6**(10): e202302100.

Ballow D, Meistrich ML, Matzuk M, et al. 2006. *Sohlh1* is essential for spermatogonial differentiation. *Developmental Biology*, **294**(1): 161–167.

Beckers A, Adis C, Schuster-Gossler K, et al. 2020. The *FOXJ1* target *Cfap206* is required for sperm motility, mucociliary clearance of the airways and brain development. *Development*, **147**(21): dev188052.

Bertho S, Pasquier J, Pan QW, et al. 2016. *Foxl2* and its relatives are evolutionary conserved players in gonadal sex differentiation. *Sexual Development*, **10**(3): 111–129.

Blay C, Planes S, Ky CL. 2017. Donor and recipient contribution to phenotypic traits and the expression of biomineralisation genes in the pearl oyster model *Pinctada margaritifera*. *Scientific Reports*, **7**(1): 2696.

Capt C, Renaut S, Stewart DT, et al. 2019. Putative mitochondrial sex determination in the bivalvia: insights from a hybrid transcriptome assembly in freshwater mussels. *Frontiers in Genetics*, **10**: 840.

Chassot AA, Gillot I, Chaboissier MC. 2014. *R-spondin1, WNT4*, and the *CTNNB1* signaling pathway: strict control over ovarian differentiation. *Reproduction*, **148**(6): R97–R110.

Chávez-Villalba J, Soyez C, Huvet A, et al. 2011. Determination of gender in the pearl oyster *Pinctada margaritifera*. *Journal of Shellfish Research*, **30**(2): 231–240.

Chen SF. 2023. Ultrafast one-pass FASTQ data preprocessing, quality control, and deduplication using fastp. *iMeta*, **2**(2): e107.

Chen TT, Liu Y, Song SQ, et al. 2022. Full-length transcriptome analysis of the bloom-forming dinoflagellate *Akashiwo sanguinea* by single-molecule real-time sequencing. *Frontiers in Microbiology*, **13**: 993914.

Chin CH, Chen SH, Wu HH, et al. 2014. *cytoHubba*: identifying hub objects and sub-networks from complex interactome. *BMC Systems Biology*, **8**(S4): S11.

Deng D, Xing SS, Liu XX, et al. 2022. Transcriptome analysis of sex-biased gene expression in the spotted-wing *Drosophila, Drosophila suzukii* (Matsumura). *G3 Genes| Genomes| Genetics*, **12**(8): jkac127.

Derbali A, Jarboui O, Ghorbel MH, et al. 2009. Reproductive biology of the pearl oyster, *Pinctada radiata* (Mollusca: Pteriidae), in northern Kerkennah Island (Gulf of Gabes). *Cahiers De Biologie Marine*, **50**: 215–222.

Dobin A, Davis CA, Schlesinger F, et al. 2013. STAR: ultrafast universal RNA-seq aligner. *Bioinformatics*, **29**(1): 15−21.

Domingos JA, Budd AM, Banh QQ, et al. 2018. Sex-specific *dmrt1* and *cyp19a1* methylation and alternative splicing in gonads of the protandrous hermaphrodite *Barramundi*. *PLoS One*, **13**(9): e0204182.

Doniach T & Hodgkin J. 1984. A sex-determining gene, *fem-1*, required for both male and hermaphrodite development in *Caenorhabditis elegans*. *Developmental Biology*, **106**(1): 223–235.

Elkrewi M, Moldovan MA, Picard MaL, et al. 2021. Schistosome w-linked genes inform temporal dynamics of sex chromosome evolution and suggest candidate for sex determination. *Molecular Biology and Evolution*, **38**(12): 5345–5358.

Evensen KG, Robinson WE, Krick K, et al. 2022. Comparative phylotranscriptomics reveals putative sex differentiating genes across eight diverse bivalve species. *Comparative Biochemistry and Physiology Part D: Genomics & Proteomics*, **41**: 100952.

Falcon S, Gentleman R. 2007. Using GOstats to test gene lists for GO term association. *Bioinformatics*, **23**(2): 257–258.

Fang JY, Yang CY, Liao YS, et al. 2024. Transcriptomic and metabolomic analyses reveal sex-related differences in the gonads of *Pinctada fucata martensii*. *Comparative Biochemistry and Physiology Part D: Genomics & Proteomics*, **52**: 101304.

Feng CWA, Spiller C, Merriner DJ, et al. 2017. *SOX30* is required for male fertility in mice. *Scientific Reports*, **7**(1): 17619.

Franceschini A, Szklarczyk D, Frankild S, et al. 2013. STRING v9.1: protein-protein interaction networks, with increased coverage and integration. *Nucleic Acids Research*, **41**(Database issue): D808−D815.

Froussios K, Mourão K, Simpson G, et al. 2019. Relative abundance of transcripts (*RATs*): identifying differential isoform abundance from RNA-seq. *F1000Research*, **8**: 213.

Fu X, Sun Y, Wang J, et al. 2014. Sequencing-based gene network analysis provides a core set of gene resource for understanding thermal adaptation in Zhikong scallop *Chlamys farreri*. *Molecular Ecology Resources*, **14**(1): 184–198.

Gómez-Redondo I, Planells B, Navarrete P, et al. 2021. Role of alternative splicing in sex determination in vertebrates. *Sexual Development*, **15**(5-6): 381–391.

Graham P, Penn JKM, Schedl P. 2003. Masters change, slaves remain. *BioEssays*, **25**(1): 1–4.

Gregoire EP, De Cian MC, Migale R, et al. 2023. The *-KTS* splice variant of *WT1* is essential for ovarian determination in mice. *Science*, **382**(6670): 600–606.

Gu ZF, Huang FS, Wang H, et al. 2014. Contribution of donor and host oysters to the cultured pearl colour in *Pinctada martensii*. *Aquaculture Research*, **45**(7): 1126–1132.

Guo XL, Li XX, Zhao F, et al. 2023. Full-length transcriptome analysis provides insights into larval shell formation in *Mulinia lateralis*. *Frontiers in Marine Science*, **9**: 1111241.

Haile S, Corbett RD, Leblanc VG, et al. 2021. A scalable strand-specific protocol enabling full-length total RNA sequencing from single cells. *Frontiers in Genetics*, **12**: 665888.

Haltenhof T, Kotte A, De Bortoli F, et al. 2020. A conserved kinase-based body-temperature sensor globally controls alternative splicing and gene expression. *Molecular Cell*, **78**(1): 57−69. E4.

Hart AM, Travaille KL, Jones R, et al. 2016. Western Australian silver-lipped pearl oyster (*Pinctada maxima*) Industry. Perth: Department of Fisheries.

Hartmann B, Castelo R, Miñana B, et al. 2011. Distinct regulatory programs establish widespread sex-specific alternative splicing in *Drosophila melanogaster*. *RNA*, **17**(3): 453–468.

He GX, Liu XL, Xu Y, et al. 2024. Metabolic dysfunctions in pearl oysters following recurrent marine heatwaves. *Marine Environmental Research*, **200**: 106641.

Hirst CE, Major AT, Smith CA. 2018. Sex determination and gonadal sex differentiation in the chicken model. *The International Journal of Developmental Biology*, **62**(1−2−3): 153−166.

Huang BY, Zhang LL, Tang XY, et al. 2016. Genome-wide analysis of alternative splicing provides insights into stress adaptation of the Pacific oyster. *Marine Biotechnology*, **18**(5): 598–609.

Huang X, Guo YQ, Shui Y, et al. 2005. Multiple alternative splicing and differential expression of *dmrt1* during gonad transformation of the rice field eel. *Biology of Reproduction*, **73**(5): 1017–1024.

Hwang J J. 2007. Reproductive cycles of the pearl oysters, *Pinctada fucata* (Gould) and *Pinctada margaritifera* (Linnaeus) (Bivalvia: Pteriidae) in southwestern Taiwan waters. *Journal of Marine Science and Technology*, **15**(2): 1.

Iwai T, Takahashi M, Ido A, et al. 2015. Effect of gender on Akoya pearl quality. *Aquaculture*, **437**: 333–338.

Jiang CX, Liu SL, Yang YJ, et al. 2024. Population genomic analysis reveals a polygenic sex determination system in *Apostichopus japonicus*. *iScience*, **27**(10): 110852.

Jones DB, Jerry DR, Khatkar MS, et al. 2013. A high-density SNP genetic linkage map for the silver-lipped pearl oyster, *Pinctada maxima*: a valuable resource for gene localisation and marker-assisted selection. *BMC Genomics*, **14**(1): 810.

Kaessmann H. 2010. Origins, evolution, and phenotypic impact of new genes. *Genome Research*, **20**(10): 1313–1326.

Kang YJ, Yang DC, Kong L, et al. 2017. CPC2: a fast and accurate coding potential calculator based on sequence intrinsic features. *Nucleic Acids Research*, **45**(W1): W12–W16.

Kim MA, Rhee JS, Kim TH, et al. 2017. Alternative splicing profile and sex-preferential gene expression in the female and male Pacific abalone *Haliotis discus hannai*. *Genes*, **8**(3): 99.

Kimani EN, Mavuti KM, Mukiama T. 2006. The reproductive activity of the pearl oyster *Pinctada imbricata* Röding 1798 (Pteriidae) in Gazi Bay, Kenya. *Tropical Zoology*, **19**(2): 159–174.

Kobayashi S, Yamada M, Asaoka M, et al. 1996. Essential role of the posterior morphogen nanos for germline development in *Drosophila*. *Nature*, **380**(6576): 708–711.

Koopman P. 1999. *Sry* and *Sox9*: mammalian testis-determining genes. *Cellular and Molecular Life Sciences CMLS*, **55**(6−7): 839−856.

Ky CL, Nakasai S, Molinari N, et al. 2015. Influence of grafter skill and season on cultured pearl shape, circles and rejects in *Pinctada margaritifera* aquaculture in Mangareva lagoon. *Aquaculture*, **435**: 361–370.

Lai FF, Singh A, King ML. 2012. *Xenopus Nanos1* is required to prevent endoderm gene expression and apoptosis in primordial germ cells. *Development*, **139**(8): 1476–1486.

Langfelder P, Horvath S. 2008. WGCNA: an R package for weighted correlation network analysis. *BMC Bioinformatics*, **9**: 559.

Leonard JL. 2018. Transitions Between Sexual Systems: Understanding the Mechanisms of, and Pathways Between, Dioecy, Hermaphroditism and Other Sexual Systems. Cham: Springer, 165−192.

Leung SK, Jeffries AR, Castanho I, et al. 2021. Full-length transcript sequencing of human and mouse cerebral cortex identifies widespread isoform diversity and alternative splicing. *Cell Reports*, **37**(7): 110022.

Li FH, Chen SQ, Zhang T, et al. 2024. Gonadal transcriptome sequencing analysis reveals the candidate sex-related genes and signaling pathways in the East Asian common octopus, *Octopus sinensis*. *Genes*, **15**(6): 682.

Li H. 2018. Minimap2: pairwise alignment for nucleotide sequences. *Bioinformatics*, **34**(18): 3094–3100.

Li J, Harata-Lee Y, Denton MD, et al. 2017. Long read reference genome-free reconstruction of a full-length transcriptome from *Astragalus membranaceus* reveals transcript variants involved in bioactive compound biosynthesis. *Cell Discovery*, **3**: 17031.

Li QS, Li Y, Song JY, et al. 2014. High-accuracy *de novo* assembly and SNP detection of chloroplast genomes using a SMRT circular consensus sequencing strategy. *New Phytologist*, **204**(4): 1041–1049.

Li RJ, Zhang LL, Li WR, et al. 2018. *FOXL2* and *DMRT1L* are yin and yang genes for determining timing of sex differentiation in the bivalve mollusk *Patinopecten yessoensis*. *Frontiers in Physiology*, **9**: 1166.

Li XY, Gui JF. 2018. Diverse and variable sex determination mechanisms in vertebrates. *Science China Life Sciences*, **61**(12): 1503–1514.

Li XY, Mei J, Ge CT, et al. 2022a. Sex determination mechanisms and sex control approaches in aquaculture animals. *Science China Life Sciences*, **65**(6): 1091–1122.

Li YJ, Liu LJ, Zhang LJ, et al. 2022b. Dynamic transcriptome analysis reveals the gene network of gonadal development from the early history life stages in dwarf surfclam *Mulinia lateralis*. *Biology of Sex Differences*, **13**(1): 69.

Li YP, Zhang LL, Sun Y, et al. 2016. Transcriptome sequencing and comparative analysis of ovary and testis identifies potential key sex-related genes and pathways in scallop *Patinopecten yessoensis*. *Marine Biotechnology*, **18**(4): 453–465.

Liang SS, Liu DW, Li XX, et al. 2019. *SOX2* participates in spermatogenesis of Zhikong scallop *Chlamys farreri*. *Scientific Reports*, **9**(1): 76.

Liu LJ, Liu T, Wu SX, et al. 2022. Discovery of *Nanos1* and *Nanos2/3* as germ cell markers during dcallop gonadal development. *Marine Biotechnology*, **24**(2): 408–416.

Lu YF, Liu Q, Liu KQ, et al. 2022. Identification of global alternative splicing and sex-specific splicing via comparative transcriptome analysis of gonads of Chinese tongue sole (*Cynoglossus semilaevis*). *Zoological Research*, **43**(3): 319–330.

Matson CK, Zarkower D. 2012. Sex and the singular DM domain: insights into sexual regulation, evolution and plasticity. *Nature Reviews Genetics*, **13**(3): 163–174.

Matsuda M. 2005. Sex determination in the teleost Medaka, *Oryzias latipes*. *Annual Review of Genetics*, **39**: 293–307.

Mawaribuchi S, Yoshimoto S, Ohashi S, et al. 2012. Molecular evolution of vertebrate sex-determining genes. *Chromosome Research*, **20**(1): 139–151.

Mcdougall C, Aguilera F, Shokoohmand A, et al. 2021. Pearl Sac gene expression profiles associated with pearl attributes in the silver-lip pearl oyster, *Pinctada maxima*. *Frontiers in Genetics*, **11**: 597459.

Osaki E, Nishina Y, Inazawa J, et al. 1999. Identification of a novel *Sry*-related gene and its germ cell-specific expression. *Nucleic Acids Research*, **27**(12): 2503–2510.

Ray M, Conard AM, Urban J, et al. 2023. Sex-specific splicing occurs genome-wide during early *Drosophila embryogenesis*. *eLife*, **12**: e87865.

Reon BJ, Dutta A. 2016. Biological processes discovered by high-throughput sequencing. *The American Journal of Pathology*, **186**(4): 722–732.

Rurak GM, Simard S, Freitas-Andrade M, et al. 2022. Sex differences in developmental patterns of neocortical astroglia: a mouse translatome database. *Cell Reports*, **38**(5): 110310.

Sabik OL, Calabrese GM, Taleghani E, et al. 2020. Identification of a core module for bone mineral density through the integration of a co-expression network and GWAS data. *Cell Reports*, **32**(11): 108145.

Santerre C, Sourdaine P, Martinez AS. 2012. Expression of a natural antisense transcript of *Cg-Foxl2* during the gonadic differentiation of the oyster *Crassostrea gigas*: first demonstration in the gonads of a lophotrochozoa species. *Sexual Development*, **6**(4): 210−221.

Saucedo P, Monteforte M. 1997. Breeding cycle of pearl oysters *Pinctada mazatlanica* and *Pteria sterna* (Bivalvia: Pteriidae) at Bahia de la paz, Baja California Sur, Mexico. *Oceanographic Literature Review*, **12**: 1543–1544.

She ZY, Yang WX. 2017. *Sry* and *SoxE* genes: how they participate in mammalian sex determination and gonadal development?. *Seminars in Cell & Developmental Biology*, **63**: 13−22.

Shen SH, Park JW, Lu ZX, et al. 2014. rMATS: robust and flexible detection of differential alternative splicing from replicate RNA-seq data. *Proceedings of the National Academy of Sciences of the United States of America*, **111**(51): E5593–E5601.

Shi Y, Liu WG, He MX. 2018. Proteome and transcriptome analysis of ovary, intersex gonads, and testis reveals potential key sex reversal/differentiation genes and mechanism in scallop *Chlamys nobilis*. *Marine Biotechnology*, **20**(2): 220–245.

Sinclair AH, Berta P, Palmer MS, et al. 1990. A gene from the human sex-determining region encodes a protein with homology to a conserved DNA-binding motif. *Nature*, **346**(6281): 240–244.

Southgate PC, Lucas JS. 2008. The Pearl Oyster. Oxford: Elsevier, 1−35.

Southgate PC, Strack E, Hart AM, et al. 2008. Exploitation and culture of major commercial species. *In*: Southgate PC, Lucas JS. The Pearl Oyster. Oxford: Elsevier, 303−355.

Sun L, Luo HT, Bu DC, et al. 2013. Utilizing sequence intrinsic composition to classify protein-coding and long non-coding transcripts. *Nucleic Acids Research*, **41**(17): e166.

Tang L. 2019. Circular consensus sequencing with long reads. *Nature Methods*, **16**(10): 958.

Tardaguila M, De La Fuente L, Marti C, et al. 2018. SQANTI: extensive characterization of long-read transcript sequences for quality control in full-length transcriptome identification and quantification. *Genome Research*, **28**(3): 396–411.

Teaniniuraitemoana V, Huvet A, Levy P, et al. 2014. Gonad transcriptome analysis of pearl oyster *Pinctada margaritifera*: identification of potential sex differentiation and sex determining genes. *BMC Genomics*, **15**: 491.

Teaniniuraitemoana V, Huvet A, Levy P, et al. 2015. Molecular signatures discriminating the male and the female sexual pathways in the pearl oyster *Pinctada margaritifera*. *PLoS One*, **10**(3): e0122819.

Thiel T, Michalek W, Varshney R, et al. 2003. Exploiting EST databases for the development and characterization of gene-derived SSR-markers in barley (*Hordeum vulgare* L.). *Theoretical and Applied Genetics*, **106**(3): 411–422.

Tisdell C, Poirine B. 2008. Economics of pearl farming. *In*: Southgate PC, Lucas JS. The Pearl Oyster. Oxford: Elsevier, 473−496.

Tong Y, Zhang Y, Huang JM, et al. 2015. Transcriptomics analysis of *Crassostrea hongkongensis* for the discovery of reproduction-related genes. *PLoS One*, **10**(8): e0134280.

Tranter DJ. 1958. Reproduction in Australian pearl oysters (Lamellibranchia). III. *Pinctada albina* (Lamarck): breeding season and sexuality. *Marine and Freshwater Research*, **9**(2): 191–216.

Trincado JL, Entizne JC, Hysenaj G, et al. 2018. SUPPA2: fast, accurate, and uncertainty-aware differential splicing analysis across multiple conditions. *Genome Biology*, **19**(1): 40.

Van't Hof AE, Whiteford S, Yung CJ, et al. 2024. Zygosity-based sex determination in a butterfly drives hypervariability of *Masculinizer*. *Science Advances*, **10**(18): eadj6979.

Wang B, Tseng E, Regulski M, et al. 2016. Unveiling the complexity of the maize transcriptome by single-molecule long-read sequencing. *Nature Communications*, **7**: 11708.

Wang DJ, Pan ZK, Wang GX, et al. 2022. Gonadal transcriptome analysis and sequence characterization of sex-related genes in *Cranoglanis bouderius*. *International Journal of Molecular Sciences*, **23**(24): 15840.

Wang GL, Liu FF, Xu ZC, et al. 2019a. Identification of Hc-β-catenin in freshwater mussel *Hyriopsis cumingii* and its involvement in innate immunity and sex determination. *Fish & Shellfish Immunology*, **91**: 99–107.

Wang GY, Yin HY, Li BY, et al. 2019b. Characterization and identification of long non-coding RNAs based on feature relationship. *Bioinformatics*, **35**(17): 2949–2956.

Wang YX, Yang YJ, Chen MY. 2023. Identification of sex-specific splicing via comparative transcriptome analysis of gonads from sea cucumber *Apostichopus japonicus*. *Comparative Biochemistry and Physiology Part D: Genomics and Proteomics*, **45**: 101031.

Wei HL, Li WR, Liu T, et al. 2021. Sexual development of the hermaphroditic scallop *Argopecten irradians* revealed by morphological, endocrine and molecular analysis. *Frontiers in Cell and Developmental Biology*, **9**: 646754.

Wisecaver JH, Hackett JD. 2010. Transcriptome analysis reveals nuclear-encoded proteins for the maintenance of temporary plastids in the dinoflagellate *Dinophysis acuminata*. *BMC Genomics*, **11**: 366.

Wu B, Chen X, Hu J, et al. 2024. Combined ATAC-seq, RNA-seq, and GWAS analysis reveals glycogen metabolism regulatory network in Jinjiang oyster (*Crassostrea ariakensis*). *Zoological Research*, **45**(1): 201–214.

Wu SX, Zhang Y, Li YJ, et al. 2020. Identification and expression profiles of Fox transcription factors in the Yesso scallop (*Patinopecten yessoensis*). *Gene*, **733**: 144387.

Xu R, Li Q, Yu H, et al. 2018. Oocyte maturation and origin of the germline as revealed by the expression of *Nanos-like* in the Pacific oyster *Crassostrea gigas*. *Gene*, **663**: 41–50.

Xu WT, Cui ZK, Wang N, et al. 2021. Transcriptomic analysis revealed gene expression profiles during the sex differentiation of Chinese tongue sole (*Cynoglossus semilaevis*). *Comparative Biochemistry and Physiology Part D: Genomics and Proteomics*, **40**: 100919.

Yang MQ, Shang XM, Zhou YQ, et al. 2021. Full-length transcriptome analysis of *Plasmodium falciparum* by single-molecule long-read sequencing. *Frontiers in Cellular and Infection Microbiology*, **11**: 631545.

Yao ZL, Fang QF, Li JY, et al. 2023. Alternative splicing of histone demethylase *Kdm6bb* mediates temperature-induced sex reversal in the *Nile tilapia*. *Current Biology*, **33**(23): 5057−5070. e5.

Yoshimoto S, Okada E, Umemoto H, et al. 2008. A W-linked DM-domain gene, DM-W, participates in primary ovary development in *Xenopus laevis*. *Proceedings of the National Academy of Sciences of the United States of America*, **105**(7): 2469–2474.

Zhang LL, Hou R, Su HL, et al. 2012. Network analysis of oyster transcriptome revealed a cascade of cellular responses during recovery after heat shock. *PLoS One*, **7**(4): e35484.

Zhang N, Xu F, Guo XM. 2014. Genomic analysis of the Pacific oyster (*Crassostrea gigas*) reveals possible conservation of vertebrate sex determination in a mollusc. *G3 Genes*| *Genomes*| *Genetics*, **4**(11): 2207–2217.

Zhang Q, Huang JF, Fu YT, et al. 2024. Genome-wide identification and expression profiles of sex-related gene families in the Pacific abalone *Haliotis discus hannai*. *Comparative Biochemistry and Physiology Part D: Genomics and Proteomics*, **50**: 101205.

Zhang XX, Yuan JB, Zhang XJ, et al. 2019. Genome-wide analysis of alternative splicing provides insights into stress response of the Pacific white shrimp *Litopenaeus vanname*. *Frontiers in Genetics*, **10**: 845.

Zhao L, Wang CW, Lehman ML, et al. 2018. Transcriptomic analysis of mRNA expression and alternative splicing during mouse sex determination. *Molecular and Cellular Endocrinology*, **478**: 84–96.

Zhao Y, Lu H, Yu HS, et al. 2007. Multiple alternative splicing in gonads of chicken *DMRT1*. *Development Genes and Evolution*, **217**(2): 119–126.